Universidad
Tecnológica
de Pereira

ELECTRICAL ENGINEERING MASTER'S PROGRAM

A THESIS SUBMITTED AS A PARTIAL REQUIREMENT TO RECEIVE THE DEGREE OF MASTER OF ELECTRICAL ENGINEERING

Design and Implementation of a Passivity-Based Controller to Regulate the Power Flow in a DAB of a SST

Karol Daniela López Rodríguez

Advisor
PhD. Walter Julián GIL GONZÁLEZ
Co-Advisor
PhD. Andrés ESCOBAR MEJÍA

February, 2022

*T*o GOD, the owner of my life and light of my path.
To my husband Carlos Andrés, the love of my life, my accomplice and partner of my greatest adventures.
To my children Angel David, Carlos Daniel, and Andrés Felipe, who is the engine of my existence, the reason for my constant effort, my everything.
To my parents, family, and friends for accompanying me to fulfill this dream.

Abstract

The interest in updating electrical networks and the possibility of having power semiconductor devices with better features (e.g., reliability and efficiency) have encouraged the production of elements, such as a Solid-State Transformer (SST). The SST is one of the determining elements of the smart grid since it has the functionalities of a conventional transformer and allows an appropriate integration of distributed generation sources, loads, and energy storage devices with the traditional power grid, in addition to having system functionality advantages such as unity power factor, mitigation of sags and swells, improving system efficiency and quality, and allowing a bidirectional flow of power. For this reason, the SST could replace the traditional transformer, considering the advantages it offers functional and physicals (less weight and volume). The intelligent energy management of an SST in a smart grid is feasible through the regulation of the power flow in its central device so-called Dual Active Bridge (DAB), which due to its topology (two half-bridge and a high-frequency link) make possible the bidirectionally on the power flow and permit the interconnection of renewable sources and other elements dc into a smart grid, and that in this way the advantages of SST can be made available within a power system. Hence, this work focuses on proposing a current controller based on Proportional-Integral (PI) passivity that regulates the power flow bidirectionally in a DAB. The proposed controller guarantees the system's stability in a closed-loop, maintaining its passive properties. In addition, this controller preserves the simplicity of a PI control with high performance and robustness, where its control law is simple and does not depend on the converter's parameters.The performance and effectiveness of the proposed controller are validated and compared with a conventional PI controller, through Matlab/Simulink detailed simulations and experimental implementation on a real DAB prototype, under different variations of power flow, including bidirectional power flow. The results show that the proposed controller has a better performance than the classic PI controller since the overshoots, the settling time, and the steady-state error of the output current were decreased when the proposed approach was implemented.

Acknowledgements

First of all, I would like to express my sincere gratitude to my research supervisors Ph.D. Walter Julián Gil González and Ph.D. Andrés Escobar Mejía, for his understanding, patience, guidance, unconditional support, constant advice, and above all for the shared knowledge, which was a fundamental basis for the realization of this project, it was a great pleasure to work with such knowledgeable, dedicated, and hardworking people.

I would like to thank the Power Electronics research group and especially its director Alfonso Alzate and the Universidad Tecnológica de Pereira , for providing me with an adequate space to carry out this project, and my friends and fellow members of the group, for their help and support during my research.

A special thanks to Msc. Ana Julieth Marin Hurtado for the time, the accompaniment, and the support in the final stage of this project.

Last but not least, a thank you to all the people who in one way or another were present at this stage of my life.

Table of Contents

List of Figures

Chapter 1

Introduction

1.1 Definition of the Problem

The growth of the world population and the development of new technologies mean that the demand for electrical energy also continuously increases, requiring more electrical energy generation. Usually, electric power generation is mainly produced from fossil fuel power plants, which contribute significantly to the deterioration of the ozone layer due to a large amount of polluting gases emitted into the environment (e.g., CO_2) [1–3]. Hence, it has become a necessity to find a way to include more efficient and environmentally friendly energy sources within the systems in a more significant proportion [4]. However, this power source is highly dependent on weather conditions, so it is impossible to forecast an exact amount of power generation; therefore, it can not guarantee the supply of large loads.

According to state of the art, one of the most popular solutions to get a more efficient power grid, is to bring the power generation closer to the consumption centers [5]. Hence, it is possible to supply the demand locally and improve the efficiency, reliability, and security of the electrical network [6]. The implementation of these energy sources implies the modernization of the electrical network and the transformation of its vertical operation, becoming what is currently called a smart grid. A smart grid makes it possible to interconnect distributed generation sources, different types of energy storage systems and loads, telecommunications systems, and other elements [7, 8]. Additionally, a smart grid also allows bidirectional power flows and can operate in grid-connected and -isolated mode [5].

Some of the purposes of a smart grid are to change the verticality of conventional electrical systems and increase the participation of more planet-friendly energy sources (e.g., wind, solar, geothermal, etc.), its implementation requires an adequate interaction of its elements. Furthermore, with the final purpose

to meet the growing demand, clean energy sources are strategically situated to harness the primary source [9], with the ac network, the different types of load, and the energy storage elements, this makes it necessary to use power electronic devices that allow the coexistence of both ac elements and dc elements in the system [10, 11]. With the availability of technology, different devices have been developed; one of the most prominent is the SST [12].

The topology of the SST consists of a series of converters that allow the connection of several elements between its different stages. The basic configuration of a SST, is composed of a rectifier, a dc-to-dc converter, and an inverter converter, in which the first converter (rectifier) supplies energy to a dc-to-dc converter, and this, in turn, supplies energy to the last converter (inverter). This configuration makes the SST can be interconnected to the ac grid connection, converting to the SST in a central device of a smart-grid.In addition, the SST allows managing a bidirectional energy flow, increasing/decreasing the output voltage, achieving a unity power factor, mitigating drops and swelling on both sides [13], improves energy quality and is smaller than conventional transformers; Therefore, the SST could replace them [12]. These advantages in SST are due to the high-frequency transformer that allows decoupling between the primary and secondary bridges [14].

Taking into account the importance that SST devices may have in the future of electrical systems, there are several investigations focused on improving its topology and control schemes [15–17]. The dual active bridge (DAB) is a fundamental piece for the SST operation. The DAB is a dc to dc converter made up of two h-bridges and a high-frequency link, that manages the power flow in the SST device through the phase shift between the signals to the input and output bridges [18].

Several investigations have performed different techniques to manage the power flow through the DAB converter, since traditional schemes, involving PI controllers [19–22] to implementing new methodologies such as the inclusion of master-slave schemes [23], model predictive control (MPC) [24–26], and virtual power control [27]. However, in traditional phase shift control, the power flow of DAB converters is mainly dependent on leakage inductance, causing high current levels in the converter when the voltage transfer ratio deviates significantly from the unit [28, 29], and in the modern schemes require an enormous off-line computational burden for several operating conditions and these are difficult to implement.

1.2 Justification

In accordance with the previously outlined panorama, this work focuses on designing and implementing a closed-loop controller to regulate the power flow in a DAB, which allows the SST to be the power flow manager in an smart grid, taking advantage of its bidirectionality. In order to achieve this purpose and analyzing the characteristics of the DAB dynamic model, passivity-based control (PBC), is studied as a viable option due to that the equivalent model of a DAB has a passive nature –port-Hamiltonian (pH) systems–, and for this type a systems, PBC strategy is adequate [30]. The advantage of this control methodology is that it guarantees exponential or asymptotically stability in the sense of Lyapunov under the closed-loop operation of the dynamic system [31–36]. Furthermore, these investigations show that the application of PBC theory in power electronics converters allows establishing a robustness controller on the output variables.

This project proposes a PI passivity-based current controller to regulate the power flow on a DAB, which guarantees stability in closed-loop operation and considers the non-linearity of the DAB model. It also maintains the advantages of PI controllers in terms of robustness and implementation. The proposed controller exploits the pH structure of the DAB, which in closed-loop keeps a passive structure. Furthermore, this controller maintains the output voltage levels independent of the power flow variations in the DAB. In addition, the results showed that the controller proposed can be extended for an application in real power electrical systems, as is the case of the Colombian system, where, through the Ministry of Mines and Energy, it is currently working on the "Mission of Energy Transformation [37]." The Government of Colombia is interested in structuring a proposal to modernize the electricity sector, facilitating the incorporation of new technologies such as microgrids and distributed generation. Here the SST could play a fundamental role in integrating these elements to the grid and, with the results obtained in this project, the ability to regulate the power flow in it.

1.3 Research Objectives

1.3.1 Overall objective

- Design and implement a closed-loop controller to regulate the power flow in a DAB.

1.3.2 Specific objectives

- Achieve a review of the state of the art of SST and the control methodologies used for the different stages of the same.

- Model the DAB of SST.
- Implement one of the controllers found in the literature on the DAB model.
- Design a control scheme to regulate the power flow in the DAB of an SST.
- Simulate the closed-loop controller in specialized software.
- Implement the controller on the transformer prototype.
- Perform laboratory tests for design validation.

1.4 Literature Review

The SST emerges as an alternative for the conventional transformer made up of windings and core, and that operates with a fundamental frequency of 50/60 Hz, to obtain energy conversion with a device of smaller dimension and greater efficiency [13, 14].

This concept was introduced in [38], where high-frequency conversion techniques and a solid-state component are used to achieve an ac/ac converter; this was called the electronic transformer. Considering that semiconductor devices are an essential part of SST, the evolution in the development of its topologies has been limited to the technological advances achieved in this area of knowledge. For this reason, progress towards the construction of SSTs more efficiently has been presented together with the achievements in power electronics [10, 11].

The basic configuration of the SST consist of several power converters with an isolated stage as shown in the Fig.1.1.

This configuration enables the SST to be considered a transcendental element for smart-grids, since, through its different converters, it facilitates the integration and adequate interaction of ac and dc elements as shown in the Fig.1.2,

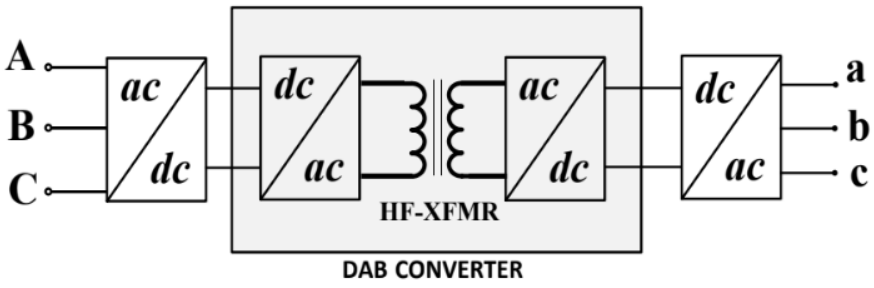

Figure 1.1: SST Topology as interface between two ac grids

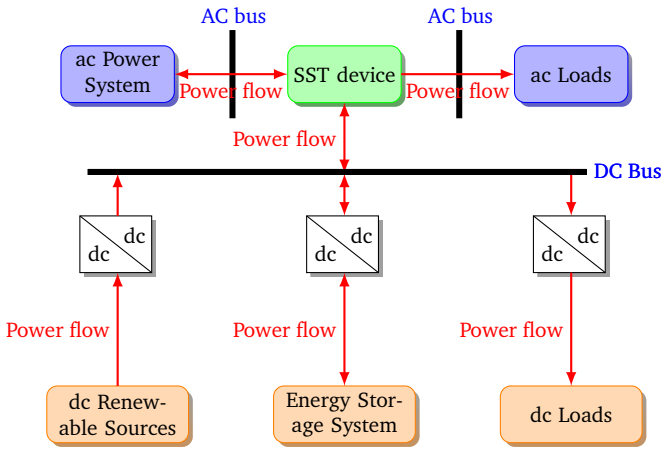

Figure 1.2: SST as a power flow manager in a smart-grid

becoming not only a link between the elements but also in a power flow manager, because, through the control phase-shifting the voltages on both sides in the central part (DAB converter) of the SST, it is possible to handle the required power levels in a bidirectional way [39].

Several investigations have performed different techniques to manage the power flow through the DAB converter, such as traditional schemes, where the power flow is controlled by the phase shift between the voltages on both sides of the DAB converter [19,20]. This method fixes one bridge while the other bridge delays or directs depending on the direction of power flow. In [21], a conventional control scheme over the H-bridges was proposed in order to solve problems of unbalanced power in the DAB. Nevertheless, the proposal was not evaluated bidirectionally. Furthermore, traditionally phase shift control schemes have in common that the voltage transfer ratio moves away from unity, the power flow through DAB chiefly depends on the leakage inductor, causing high current peaks in the converter [28,29].

In [23], a master-slave control scheme was presented to compensate for disturbances in power and voltage of the SST device. The master scheme performs all the control and modulation calculations, and with this information, the slave scheme acts on the protection and switching of the device, simplifying the general modulation algorithm. In [22] a strategy based on a PI controller was described, which allows setting voltages at the output of the converter in the desired reference. This closed-loop control scheme was able to robustly and effectively keep the desired output voltage under different load changes. However, it presented inconsistencies for references close to zero, so that in these values, it couldn't reach effectively the desired reference.

Recently, different multivariable control techniques have been also implemented for controlling DAB. Such as the model predictive control (MPC) [24–26]. Reference [18] was proposed an MPC approach under conditions of startup and reference changes for load and voltage changes. Reference, [18] showed that it is possible to improve the efficiency and dynamic response of the DAB via a dual-phase shift (DPS), applied to the MPC. However, the predictive current control is sensitive to the parameter variations which is not suitable for high-frequency applications.

Other modern concepts have been investigated, such as virtual power control plus a PI controller. In [27] presented that it is possible to achieve the desired output power and enhance the dynamic response of the DAB converter at the same time. In [40] and [41] were proposed a PI controller which uses previous operating conditions to establish different functions. These functions calculate the necessary phase-shift control for an adequate operation. However, these previous investigations do not consider the bidirectionally of the converter, and their implementation is also difficult since they need to evaluate different off-line operating conditions, which implies a high computational cost. Unlike previous investigations, this paper proposes a PI controller based on passivity theory to control the bidirectional power flow on a DAB.

1.5 Contributions

This project developed a passivity-based current controller to the DAB of a solid-state transformer. The current controller allowed managing the power flow in the DAB in a bidirectional way, considering the DAB model's passive behavior as a port-Hamiltonian system, which guarantees an asymptotic or exponential stability in itself. In this context, this passivity-based controller can be used as a fundamental part of a smart-grid management system, allowing the SST to be the regulator of power flow and integrator of clean energy sources and energy storage to work together with the conventional ac network.

As a consequence of this project and the achieved results, the following knowledge products were developed:

- Conference paper: "*Passivity-Based Current Control of a Dual-Active Bridge to Improve the Dynamic Response of a Solid-State Transformer During Power and Voltage Variations*," K. López-Rodríguez, A. Escobar-Mejía, E. Y. Piedrahita-Echavarria and W. Gil-González, 2020 IEEE 11th International Symposium on Power Electronics for Distributed Generation Systems (PEDG), 2020, pp. 230-235, DOI: 10.1109/PEDG48541.2020.9244412. **https://ieeexplore.ieee.org/document/9244412**

- Journal paper: "D*esign and Implementation of a Passivity-Based PI Controller to Regulate the Power Flow in a DAB of a SST*," K. López-Rodríguez,

A. Escobar-Mejía and W. Gil-González (in Review). **Results in Engineering (Q2)**

1.6 Document structure

The document of this degree work is developed in five chapters, which are described below:

Chapter one presented the introduction, where the definition of the problem that motivated the development of this research is presented, the justification for using the passivity-based controller to solve the problem of power flow regulation in a DAB, a literature review, the objectives of this project, and contributions to the investigation.

Later in chapter two, the DAB's detailed model is presented, where its behavior is analyzed as a port-Hamiltonian system and, therefore, like a passive model.

Chapter three shows in detail, the development of the passivity based current controller proposed in this project.

In chapter four, the validation tests carried out by simulation and experimentation for the PI passivity-based current controller are shown in comparison with a classic PI controller, under different operating conditions, i.e. to different power flow requirements.

Finally, conclusions and the proposals for future work are presented in chapter five.

Chapter 2

Dynamical Model of a DAB

2.1 DAB Model

The DAB is an isolated bidirectional dc to dc converter, which topology consists of two half-bridges, one on the input (primary) and one on the output (secondary) side, respectively; and a high-frequency transformer (with turn ratio 1:n). The transformer provides galvanic isolation and energy delivery through its windings. Fig. 2.1 depicts the topology of a DAB and its main parameters are listed in Table 2.1.

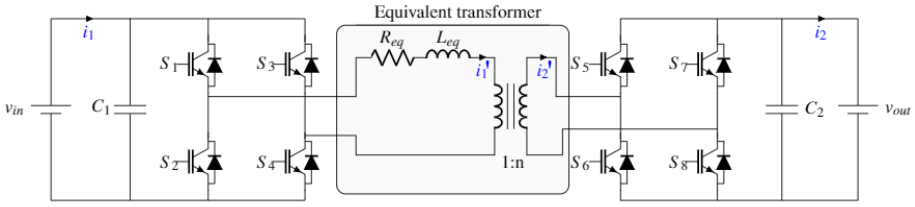

Figure 2.1: The DAB Topology

Table 2.1: DAB parameter description

Variable	Description
C_1	Input capacitor
C_2	Output capacitor
L_{eq}	Equivalent leakage inductance
R_{eq}	Equivalent winding resistance and IGBT's turn-on resistance
v_{in}, v_{out}	Input and output voltage sources
S_i	IGBTs

In this study, a reduced DAB model is considered, i.e., the magnetization branch is neglected. Despite this, the DAB model continues presenting high precision and it has an advantage for the designed controller that it will be simpler. [42, 43].

In the DAB converter, the bridges produce square wave voltages with a 50% duty cycle and these signals are applied to the transformer windings. The voltage signal on the secondary side has a phase-shift with respect to the signal on the primary side as shown in Fig. 2.2, where the IGBT's signals and transformer voltages are shown, respectively.

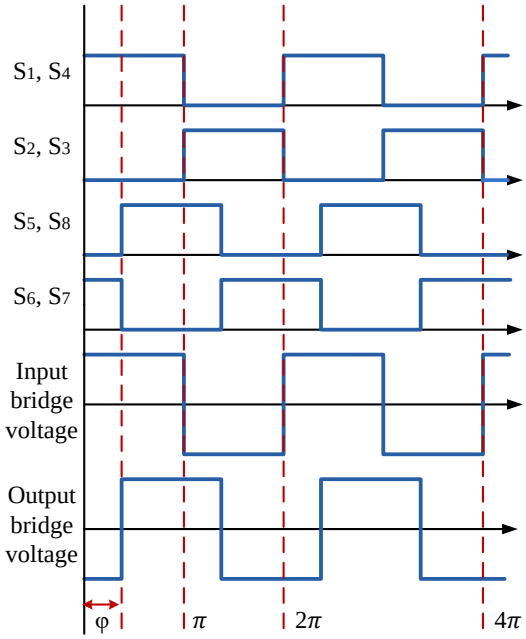

Figure 2.2: Waveforms of IGBT's switching signals and transformer voltages

According to the phase-shift between the driving signals of the two bridges, the power transfer is determined and may be calculated by (2.1),

$$P = \frac{v_{in} v_{out}}{n \omega L_{eq}} u, \tag{2.1}$$

where, n is the turns ratio of high-frequency transformer and $\omega = 2\pi f$, is radial frequency as a function of system switching frequency, f and,

$$u = \phi \left(1 - \frac{|\phi|}{\pi}\right), \tag{2.2}$$

where ϕ is the phase-shift ratio in radians of the switching signals between primary and secondary bridges [42].
By applying the first Kirchhoff's law, the DAB dynamic model can be obtained, as follows

$$\begin{aligned} C_1 \frac{dv_{c1}}{dt} &= i_1 - i_1' \\ C_2 \frac{dv_{c2}}{dt} &= -i_2 + i_2' \end{aligned} \tag{2.3}$$

where i_1 and i_2 are the input and output currents of the DAB converter, respectively. i_1' and i_2' are the input and output currents of the high frequency transformer, respectively. v_{c1} and v_{c2} are the voltages across capacitors C_1 and C_2, respectively.
Taking into account that the equivalent resistance of the high-frequency transformer is close to zero, an ideal model is considered, i.e, without losses. Thus, it can be defined,

$$\begin{aligned} P_1 &= P_2 \\ v_1 i_1' &= v_2 i_2' \end{aligned} \tag{2.4}$$

where, P_1 and P_2 are the input and output power of the transformer, respectively.
From the equation presented in (2.4), it is possible to express the input and output currents of the high-frequency transformer as follows,

$$\begin{aligned} i_1' &= \frac{v_{c2}}{n\omega L_{eq}} u, \\ i_2' &= \frac{v_{c1}}{n\omega L_{eq}} u. \end{aligned} \tag{2.5}$$

Therefore, by replacing (2.5) into (2.6), the dynamic model of DAB can be expressed as

$$\begin{aligned} C_1 \frac{dv_{c1}}{dt} &= i_1 - \frac{v_{c2}}{n\omega L_{eq}} u \\ C_2 \frac{dv_{c2}}{dt} &= -i_2 + \frac{v_{c1}}{n\omega L_{eq}} u \end{aligned} \tag{2.6}$$

2.2 DAB Model as a Port-Hamiltonian System

he theory of port-Hamiltonian (pH) systems present a framework for the geometric description of network models of physical systems [44]. PH models provide a suitable representation of many physical processes and have the essential

feature of underscoring the importance of the energy function, the interconnection pattern and the dissipation of the system [45].

The great advantage of the pH description of physical systems is that it highlights all the energetic properties of the system, and allows a representation to be given based on its behavior. In this way, dynamic systems with similar behavioral characteristics can be modeled in the same way, thus, results obtained on port-Hamiltonian physical systems, such as effective control techniques, to be extended to other systems that can be similarly described [44, 45].

The dynamic model of the DAB system (2.6) can be rewritten as a pH system [44–46], as follows

$$Q\dot{x} = (Ju - R)\, x + d, \tag{2.7}$$

with $x = [v_{c1},\ v_{c2}]^\top$, $d = [i_1,\ i_2]^\top$,

$$Q = \begin{bmatrix} C_1 & 0 \\ 0 & C_2 \end{bmatrix},\ J = \begin{bmatrix} 0 & -\frac{1}{a} \\ \frac{1}{a} & 0 \end{bmatrix},\ R = \begin{bmatrix} 0 & 0 \\ 0 & 0 \end{bmatrix}$$

where $a = n\omega L_{eq}$, x is the state vector and d corresponds to the external input-vector and u is the control signal. $Q = Q^\top \succ 0$ is known as the inertia matrix, and $J = -J^\top$ is the interconnection matrix, which is knew-asymmetric.

Chapter 3

PI Passivity-Based Control

3.1 Port-Hamiltonian Passive System

The dynamic systems with a port-Hamiltonian structure are suitable to design their control with theory based on passivity. The passivity-based control (PBC) is a robust non-linear control theory and is well-known for its efficiency because this theory guarantees the stability exponentially or asymptotically in the Lyapunov sense under closed-loop operation of the dynamic system [31–35], [47].The PBC has different strategies to deal with a subclass of nonlinear systems called "bilinear systems", however, the PI-PBC is more appropriate, since to the dynamic characteristics of its structure, by unifying the PI control with the theory PBC, the convergence of the system state variables towards the desired values is accelerated, while maintaining the simplicity of the controller design. In addition, the PI gains allow eliminating the steady-state errors with the certainty that the closed-loop dynamic system will be asymptotically stable. [30].

The pH system (2.7) has an assignable equilibrium point $x^\star$, if satisfies the following expression,

$$Q\dot{x}^\star = (Ju^\star - R)\, x^\star + d, \tag{3.1}$$

with some bounded $u^\star$. This means that the equilibrium point $x^\star$ will be reached if exists any $u^\star$ that generates it.

The pH system (2.7) can be represented as an incremental model [46], by defining the incremental variables as $\tilde{x} = x - x^\star$ and $\tilde{u} = u - u^\star$, as follows

$$Q(\dot{\tilde{x}} + \dot{x}^\star) = (J(\tilde{u} + u^\star) - R)\,(\tilde{x} + x^\star) + d, \tag{3.2}$$

and replacing (3.1) in (3.2) yields

$$Q\dot{\tilde{x}} = (Ju^\star - R)\,\tilde{x} + Jx^\star\tilde{u}. \tag{3.3}$$

The dynamic incremental model shown in (3.3) is passive if output function

$$y = Cx = (x^\star)^\top Jx, \tag{3.4}$$

satisfies the dissipation inequality $\dot{H} \leq \tilde{y}^\top\tilde{u}$, where $\tilde{y} = y - y^\star$ with $y^\star = Cx^\star$.

Defining a storage function for the dynamic incremental model (3.3), as follows

$$H(\tilde{x}) = \frac{1}{2}\tilde{x}^\top Q\tilde{x}, \tag{3.5}$$

and taking the time derivative of $H(\tilde{x})$, as follows

$$\begin{aligned}
\dot{H}(\tilde{x}) &= \tilde{x}^\top Q\dot{\tilde{x}} \\
\dot{H}(\tilde{x}) &= \tilde{x}^\top\left[(Ju^\star - R)\,\tilde{x} + Jx^\star\tilde{u}\right] \\
\dot{H}(\tilde{x}) &= -\tilde{x}^\top R\tilde{x} + \tilde{x}^\top Jx^\star\tilde{u} \\
\dot{H}(\tilde{x}) &\leq \tilde{x}^\top Jx^\star\tilde{u} = \tilde{y}^\top\tilde{u},
\end{aligned} \tag{3.6}$$

therefore, this demonstrates that the dynamic incremental system (3.3) is passive.

3.2 PI-PBC Controller Design and Stability Analysis

Let us consider that the pH system described by (2.7) in a closed-loop has an admissible equilibrium point $x^\star$ with the following PI controller [48]:

$$\begin{aligned}
\dot{z} &= -\tilde{y} \\
\tilde{u} &= -K_p\tilde{y} + K_i z,
\end{aligned} \tag{3.7}$$

with $K_p \succ 0$ and $K_i \succ 0$ furthermore, for any initial conditions the trajectories of the closed-loop system are bounded.

In order to demonstrate the stability of the dynamical system given by (3.1), it defines the following Lyapunov candidate function:

$$W(\tilde{x}, z) = H(\tilde{x}) + \frac{1}{2} z^\top K_i z. \tag{3.8}$$

It can observe that $W(0,0) = 0 \; \forall x = x^\star$ and $W(\tilde{x}, z) > 0 \; \forall x \neq x^\star, \; z \neq 0 \in \mathbb{R}^n$, and thus, the first two Lyapunov conditions are satisfied [49].

Taking the time derivative of $W(\tilde{x}, z)$ and considering (3.2),

$$\begin{aligned} \dot{W}(\tilde{x}, z) &= \dot{H} + z^\top K_i \dot{z} \\ \dot{W}(\tilde{x}, z) &= -\tilde{x}^\top R \tilde{x} + \tilde{y}^\top \tilde{u} + z^\top K_i (-\tilde{y}) \\ \dot{W}(\tilde{x}, z) &\leq \tilde{y}^\top \tilde{u} + (\tilde{u} + K_p \tilde{y})^\top (-\tilde{y}) = -\tilde{y}^\top K_p \tilde{y} \leq 0, \end{aligned} \tag{3.9}$$

hence, it proves that the dynamic system (2.7) is stable and x converges to $x^\star$.

3.3 DAB Controller Design

Using (3.4) is computed the passive output for the DAB system as

$$y = \frac{1}{a}[x_1^\star x_2 - x_2^\star x_1]. \tag{3.10}$$

The admissible equilibrium point of the dynamic system (2.7) is achieved employing the following control input (3.11), which was calculated from (3.1), when the system goes in a steady-state condition, i.e., if $x^\star$ is constant and $Q\dot{x}^\star = 0$.

$$u^\star = \frac{a i_2^\star}{x_1^\star}, \tag{3.11}$$

where, $i_2^\star$ and $x_1^\star$ are the desired equilibrium points for i_2, and v_{c1}, respectively.

Notice that i_2 is not a state variable, however, it is a variable dependent on the dynamics of the system, therefore when desired values are assigned to the output current, indirect control over the states is being performed.

Now, the proposed controller for DAB is defined as:

$$u = u^\star + \tilde{u}, \tag{3.12}$$

and finally, the phase-shift is calculated from the control signal u, considering in (2.2), as follows

$$\phi = \begin{cases} \dfrac{-\pi + \sqrt{\pi^2 + 4u\pi}}{2}, \ if \ u < 0, \\ \dfrac{\pi + \sqrt{\pi^2 - 4u\pi}}{2}, \ if \ u > 0, \end{cases} \tag{3.13}$$

where, u is a boundary function, $-\dfrac{\pi}{4} \leq u \leq \dfrac{\pi}{4}$.
The passivity-based controller schematic for the DAB is presented in Fig. 3.1. It is possible to observe that the control signal u, is calculated from the sum of three different functions, the first function considers the desired equilibrium points $i_2^\star$, $x_1^\star$ and the necessary conditions for the system to be in a steady-state. The second function, considers the output that guarantees the passivity of the system y and a proportional gain K_p, and the third function is calculated from the integral of the output system y and its corresponding gain K_i. Once the control function has been found, it is necessary to calculate the corresponding phase-shift, depending on the value u, if $u > 0$ the phase-shift is calculated with the upper ϕ function and otherwise $u < 0$ the phase-shift is calculated with the lower ϕ function. Then, this value of ϕ is applied to the switching signals, in such a way that the system variables reach the desired equilibrium points.

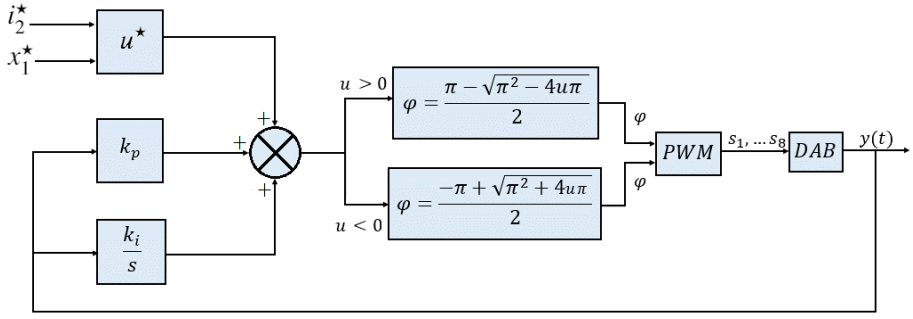

Figure 3.1: Passivity-based controller schematic

Chapter 4

Simulations and Experimental Results

In order to evaluate the proposed control design a comparison analysis is performed against a classic PI controller. Simulations and experimental results are implemented to assess the performance of the proposed PI-PBC approach. The simulations are carry out in the time-domain in Matlab/Simulink. While experimental results are performed using a real-time controller integrated on a Texas Instruments C2000 Delfino microcontroller LAUNCHXL-F28379D. It is a microprocessor that can perform data processing in real-time, which provides 800MIPS total system performance between dual 200MHz C28x CPU and dual 200MHz real-time control (RLA) coprocessor. The DSP, is used to generate the PWM switching signals sent to the gate drivers of IGBT's from the designed passive controller for a specific reference current considering the required power flow in the system. The objective is to obtain an adequate commutation of the semiconductor devices from the code that includes the DSP's ePWM, ADC, and DAC ports. To carry out the implementation, the DAB prototype resulting from a previous project was used, which was developed by the power electronics research group, [50]. In addition, all experiments were carried out in the Power Electronics Laboratory of the Technological University of Pereira. The DAB prototype and the elements used for the implementation are shown in Figs. 4.1 and 4.2 and the system parameters are listed in Table 4.1.

According to the topology of the DAB converter analyzed in the previous chapters, in the Figs. 4.1 and 4.2 it can observe the different devices that were used to carry out the implementation. Two sources Gw instek psw (model 160V - 21.6A 4.1 (b) and 800V - 4.32A 4.1 (c)) were used to supply the input and output voltages of the converter respectively, which were voltage controlled by an external dual-source Bk precision 1652 4.1 (e), in order for the capacitors could be progressively charge at the same time.

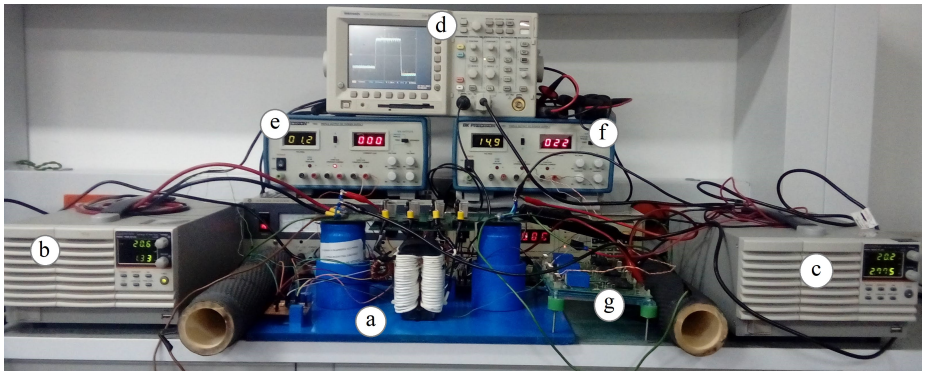

Figure 4.1: Front view of the experimental setup: a) DAB prototype, b) DC input source, c) DC output source, d) Oscilloscope, e) DC source to control voltage on input/output sources, f) Power supply for the voltage sensors, and g) Voltage sensors.

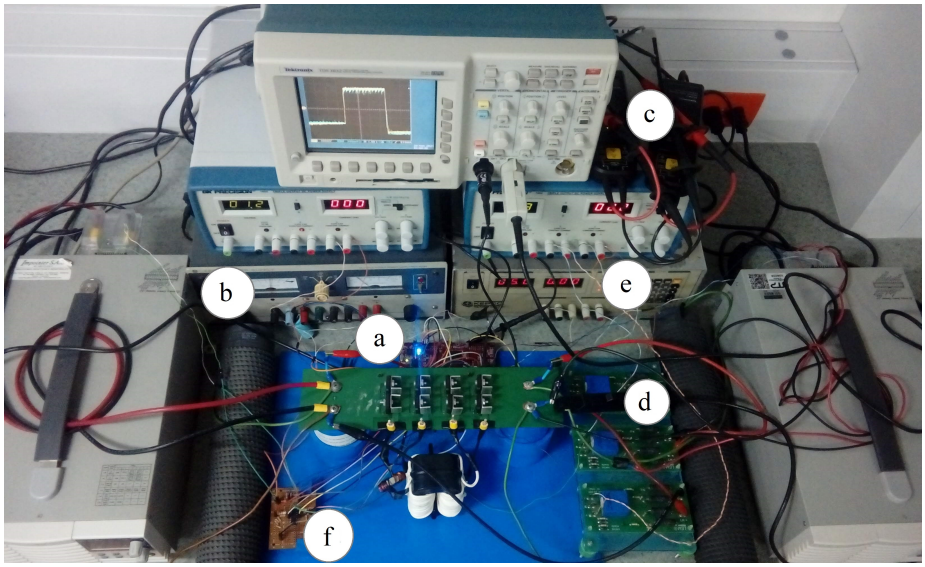

Figure 4.2: Plant view of the experimental setup: a) DSP LAUNCHXL-F28379D C2000 Delfino MCUs, b) Gate drivers power supply, c) Voltage differential probes, d) Current probe, e) Signal conditioning source, and f) Signal conditioning circuit.

Table 4.1: System Parameters

Parameter	Description	Type/Value
v_{in}, v_{out}	Input/Output Voltage	20 V
f_{sw}	Switching Frequency	10 kHz
S_i	IGBT's	IRG7PH46UDPBF 1200 V, 40 A
C_1, C_2	Aluminum Electrolytic Capacitors	Cornell Dubilier 2700 μ f , 420 V
Transformer	Core	Amorphous 2505SA1 C, AMCC-80
	Cable	Wire Lizt 20 Strands 14 AWG
	Power Transfer	Ferrite T68
	Inductor	No.5968021001
	Equivalent Parameters	R_{eq} =0.1 mΩ, L_{eq} = 100 μ H
	Turns ratio	1:1
K_p	Proportional gain	1^{-6}
K_i	Integral gain	0.1^{-6}

In addition, to obtain real-time measurements of the state variables for the PI-PBC implementation, LEM LV 25mA - 400V voltage sensors were used 4.1 (g), which were powered by a Bk precision 1652 voltage source 4.1 (f). Through a signal conditioning circuit 4.2 (f), these measurements were transformed to values between 0 - 3V which were delivered to the DSP 4.2 (a)through the ADC ports. Notice, that in both figures it is possible to observe two resistive loads in parallel with the input and output voltage sources respectively, these ceramic loads (10 Ω, 1000W) were used as a safety load for the voltage sources since according to the power requirements in the system one of the two sources behaved as a sink.In order to carry out the implementation of the classic PI, to measure the DAB output current, a LEM current sensor (LA 55-P) was used, whose sensed measurement into an ADC port of the DSP as a voltage value between 0 - 3V, guaranteed by a signal conditioning circuit.

The passivity-based controller is tested under three scenarios that allow evaluating the bidirectionality of the power flow of the DAB. The power flow management is computed using the DAB's output current, which is arbitrarily assigned as shown in Table 4.2. Notice that these references are selected so that the power flow transfer is bidirectional. As mentioned, the proposed controller is compared with a classical PI controller, which gains are tuned using a linearization of the DAB model. These gains present the following values: $k_p = 5.794 \times 10^{-5}$ and $k_i = 5.79 \times 10^{-12}$.

Table 4.2: Changes of the current reference

Scenario	Power Transfer (%) (Respect to the Maximum Value)	Time (ms)
1	60% (Absorbed)	0 - 40
2	80% (Supplied)	40 - 70
3	90% (Absorbed)	70 - 100

According to Table 4.2, when the power is absorbed, the current direction is from the secondary side to the primary side, and when the power is supplied, the current direction is from the primary side to the secondary side, as shown in the Fig. 4.3.

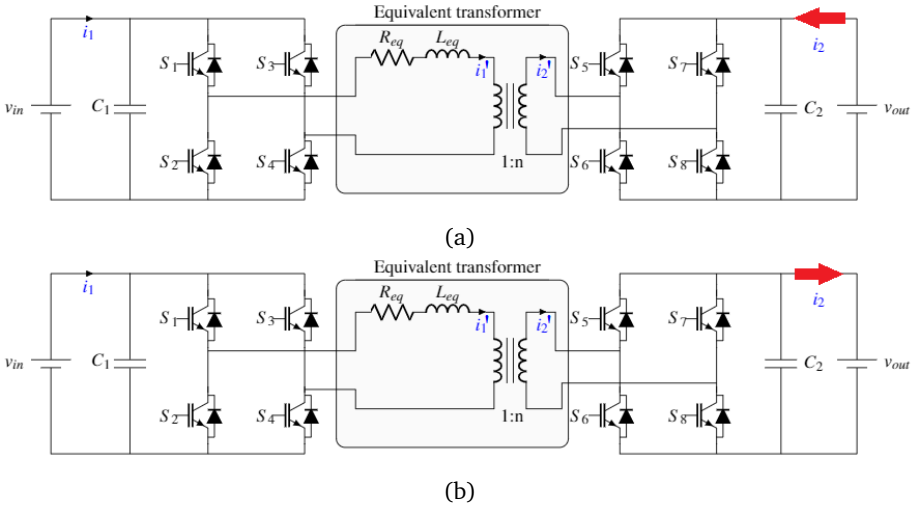

Figure 4.3: Current direction: (a) Power transfer absorbed (b) Power transfer supplied

Initially, a frequency domain analysis is carried out to evaluate the performance of both controllers. The Bode diagrams are obtained using the output-current control for the PI-PBC and PI controller based on the transfer functions (4.1) and (4.2) determined for each controller in closed-loop, respectively under Matlab/Simulink simulations.

$$H(s) = \frac{-1.451s^4 + 1395s^3 + 1.374 \times 10^6 s^2 + 7.932 \times 10^8 s - 2.462 \times 10^{10}}{s^4 + 1080s^3 + 1.077 \times 10^6 s^2 + 6.687 \times 10^8 s + 6.261 \times 10^{10}} \tag{4.1}$$

$$H(s) = \frac{-71310s^2 - 2.683 \times 10^7 s + 2.734 \times 10^{11}}{s^3 + 9952s^2 + 1.679 \times 10^7 s + 3.742 \times 10^{10}} \tag{4.2}$$

Fig. 4.4 shows the bode diagram for the PI-PBC approach (4.1), here is observed a gain margin of 8.11 dB and the phase margin from the bound of 180^o is -112^o. In Fig. 4.5 is represented the bode diagram for classical PI by (4.2), in this case, the gain margin is -21 dB, and the phase margin from the bound of 180^o is -82^o. The main conclusion in Figs. 4.4 and Figs. 4.5 is that the PI-PBC approach generates greater stability-margins, than the classical PI controller. Furthermore, according with the analysis, The PI-PBC has a stable behavior for any frequency, which is consistent with the stability concept of the proposed controller. While, the classical PI is stable in limited frequency ranges, in this case between 600Hz and 11.3 kHz.

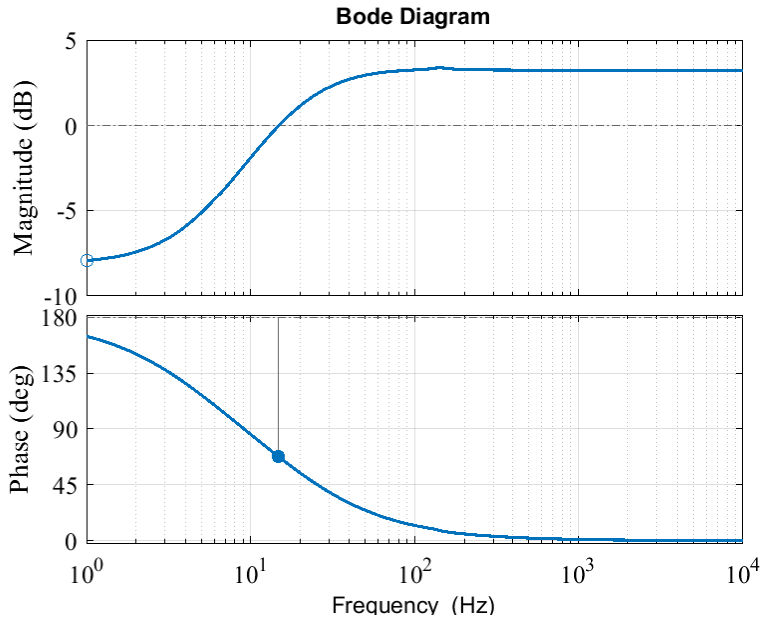

Figure 4.4: Bode diagram for the DAB by PI-PBC approach

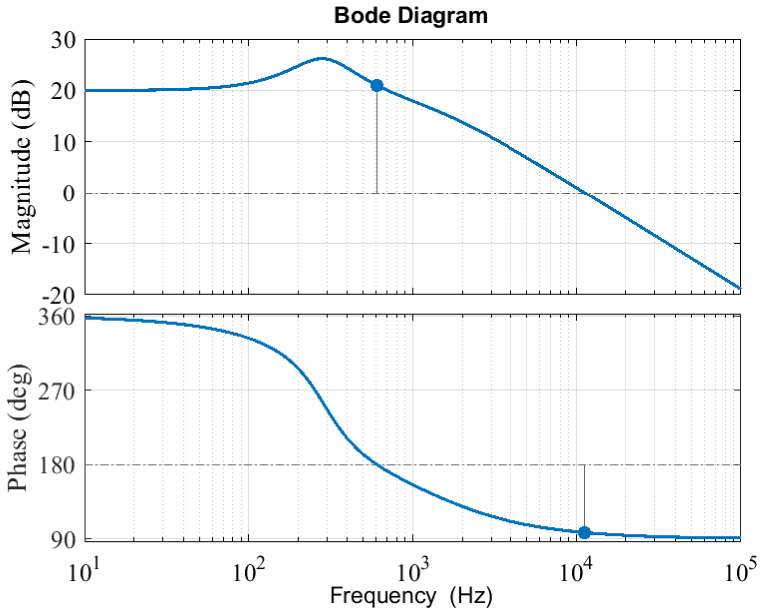

Figure 4.5: Bode diagram for the DAB by Classical PI controller

From Figs. 4.6 to 4.9 shows the detailed simulated and experimental results of the output current of the DAB using the current reference presented in Table 4.2. Figs. 4.6 and 4.7 correspond to simulation results when the PI-PBC and classical PI approaches are implemented, respectively. While Figs. 4.8 and 4.9 present the same scenarios for the experimental results. In Figs. 4.8 and 4.9, it is essential to clarify that the reference value (CH1) for the DAB's output current is presented in units of mV since this value is extracted from the DSP LAUNCHXL-F28379DC2000 Delfino MCUs as a voltage value, due to its performance characteristics. Table 4.3 lists the overshoot and settling time of the output current of the DAB for each scenario.

Notice, in Figs. 4.6 and 4.7 that the proposed PI-PBC controller has better performance than the classic PI controller. This is supported by comparing the overshoots for the DAB's output current and its settling times which are reduced by 15 % and 2 ms, and the steady-state error by 6 % in the worst scenario (see Table 4.3) when the proposed controller is used. For experimental results, the proposed controller continues presenting a better performance as shown in Fig. 4.8 and 4.9. The overshoot and settling time are reduced by 15 % and 6 ms, and the steady-state error by 6 % in the worst scenario (see Table 4.3) when the PI-PBC approach is implemented.

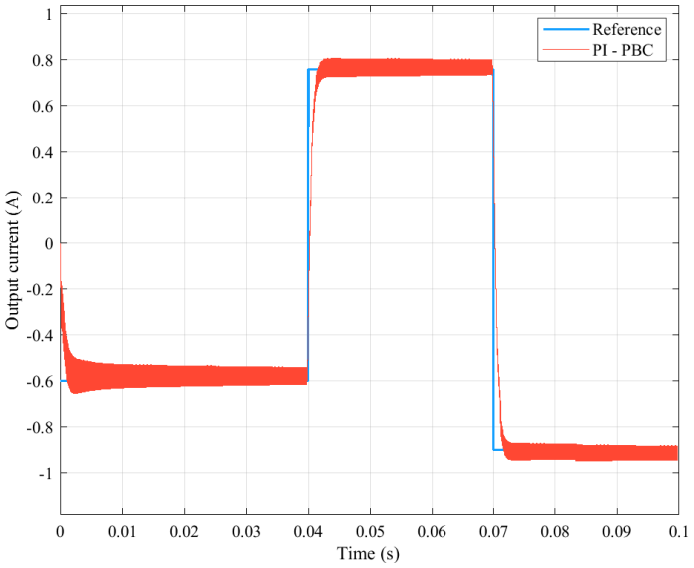

Figure 4.6: Simulated dynamic responses of the output current for DAB device by PI-PBC approach

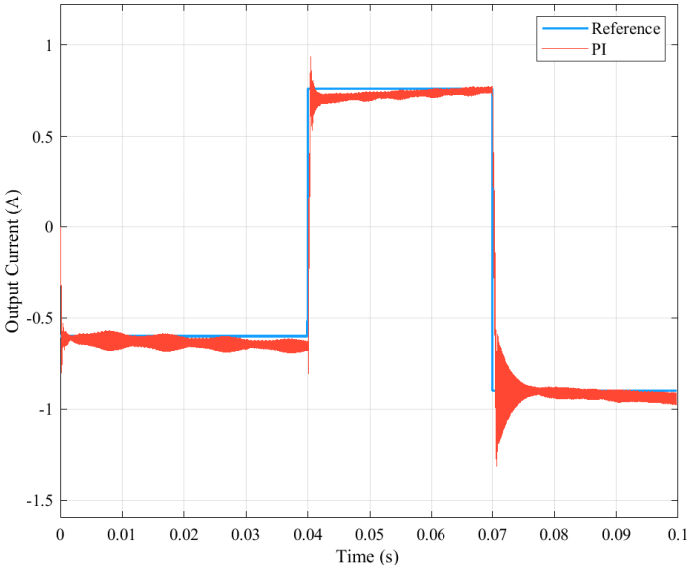

Figure 4.7: Simulated dynamic responses of the output current for DAB device by Classical PI

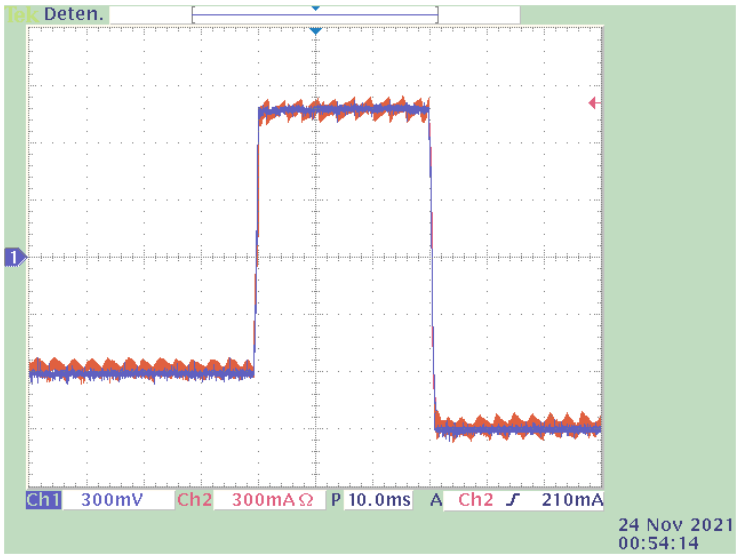

Figure 4.8: Experimental dynamic responses of the output current for DAB device by PI-PBC approach, output current (red) and reference (blue). CH1: $i_2^\star$ (300 mV/div), CH2: i_2 (300 mA/div), and time base of 10ms.

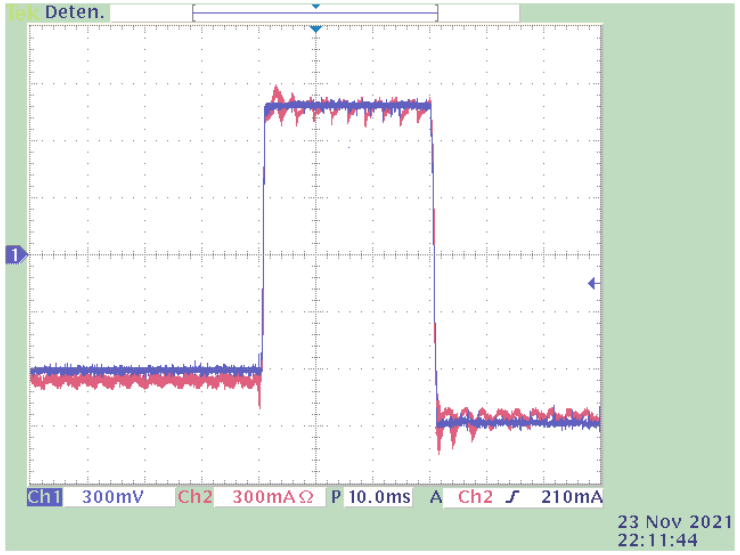

Figure 4.9: Experimental dynamic responses of the output current for DAB device by classical PI, output current (red) and reference (blue). CH1: $i_2^\star$ (300 mV/div), CH2: i_2 (300 mA/div), and time base of 10ms.

Table 4.3: Output current analysis respect to reference for the detailed simulations and experimental results

	Overshoots (%)			Settling Time (ms)			Steady-state Error (%)		
Scenarios	**1**	**2**	**3**	**1**	**2**	**3**	**1**	**2**	**3**
Simulation results									
PI-PBC	7	1	1	1	1.5	2	4	0	0.5
Classical PI	33	15.4	44	1.5	2.5	4	8	2	6
Experimental results									
PI-PBC	5	1	2	-	1	1	4	0	1
Classical PI	32.5	15.4	17	-	5	7	10	4	6

Figs. 4.10 to 4.12 illustrate the phase-shifts between the switching signals for the input and output voltages of the DAB system for experimental results, in every scenario. Figs. 4.10(a), 4.11(a), and 4.12(a) depict input/output voltages of the DAB system for experimental results when the PI-PBC approach is used. While Figs. 4.10(b), 4.11(b), and 4.12(b) show the same voltage when the classic PI controller is employed.

In the Table. 4.4, the phase-shift for both controllers in each scenario are compared, since the experimental results in Figs. 4.10 to 4.12. Observe in Figs. 4.10 to 4.12 that input/output voltages of the DAB system for both controllers present a similar behavior (see Table. 4.4); however, the output current behaviors are different as presented in Fig. 4.6. This entails that a minimal difference in the input/output voltages of the DAB system may change its performance drastically.

Additionally, observe for both controllers in the figure that the voltage at the input and at the transformer's output has a drop voltage, which can be noted in the upper part of the wave. This drop voltage is due to the IGBT's presented a conduction voltage of, which is around 2V, presenting a voltage drop at the transformer input around 4V.

Table 4.4: Phase-shift comparison between both controllers for each scenario.

μlticolumn3c**Phase-shift (degree)**		
Scenarios	**PI-PBC**	**Classical PI**
1	-51.84°	-54.72°
2	88.56°	86.4°
3	-74.16°	-72°

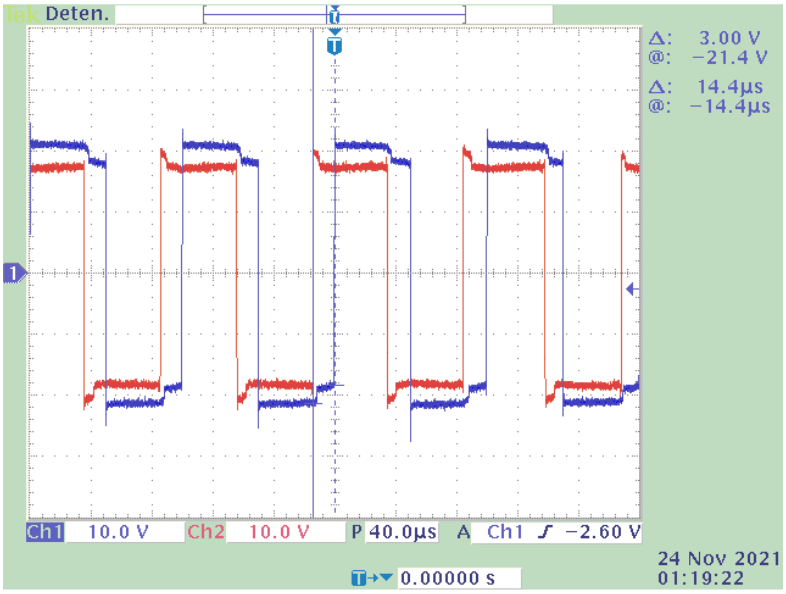

(a)

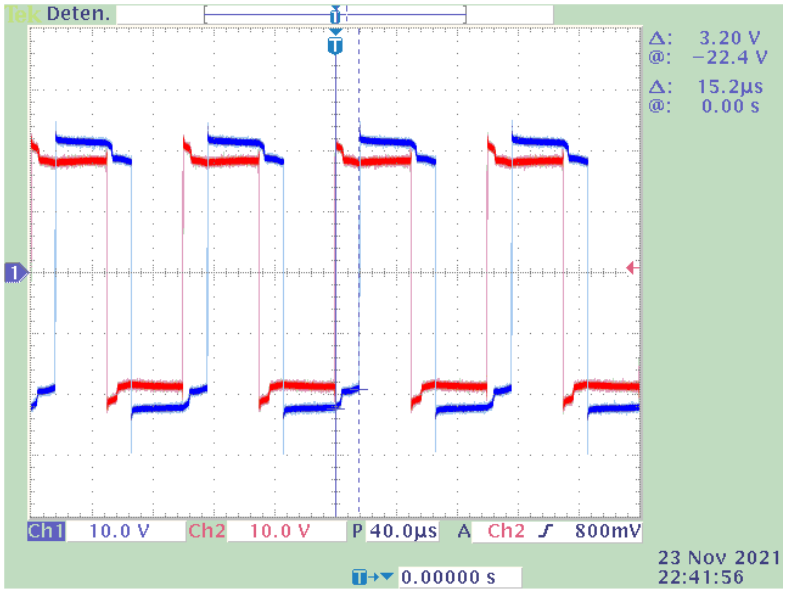

(b)

Figure 4.10: Transformer input (blue) and output (red) voltage for scenario 1: (a) PI-PBC approach, (b) Classical PI. CH1: 10V/div, CH2: 10V/div, and time base of 40 μ s.

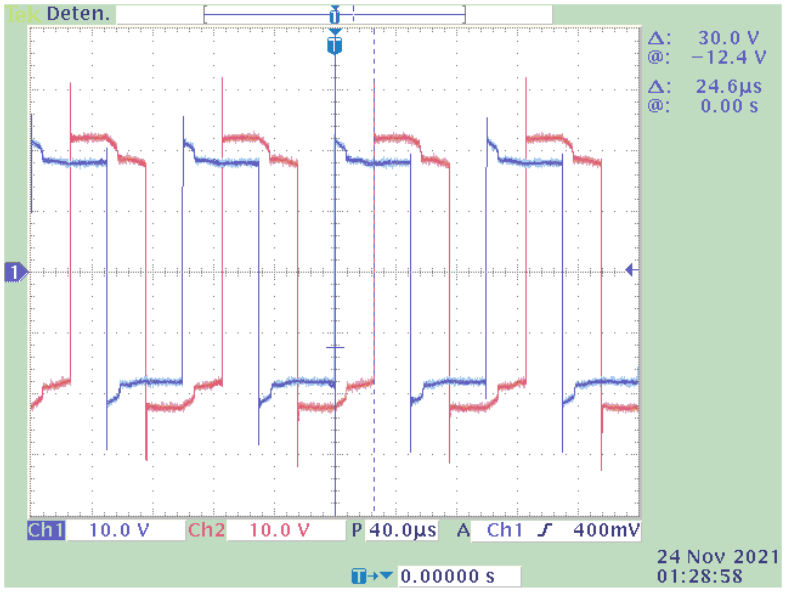

(a)

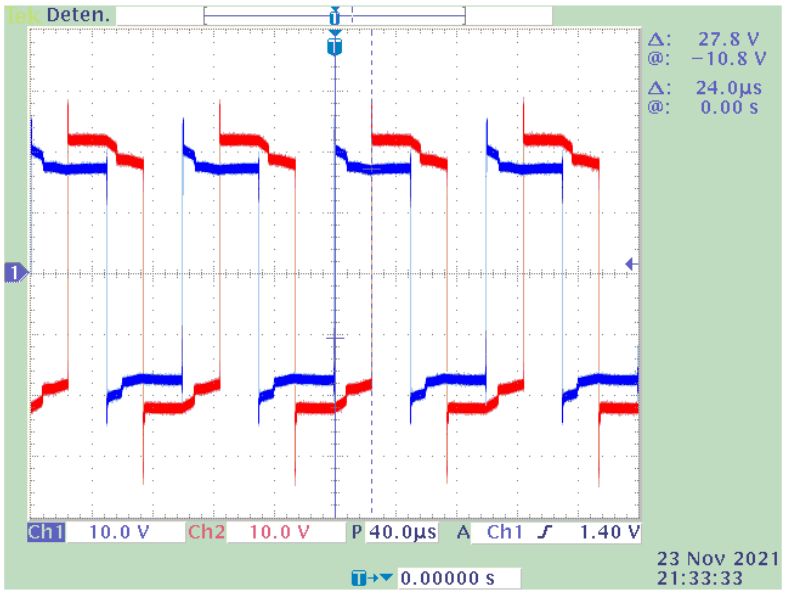

(b)

Figure 4.11: Transformer input (blue) and output (red) voltage for scenario 2: (a) PI-PBC approach, (b) Classical PI. CH1: 10V/div, CH2: 10V/div, and time base of 40 μ s.

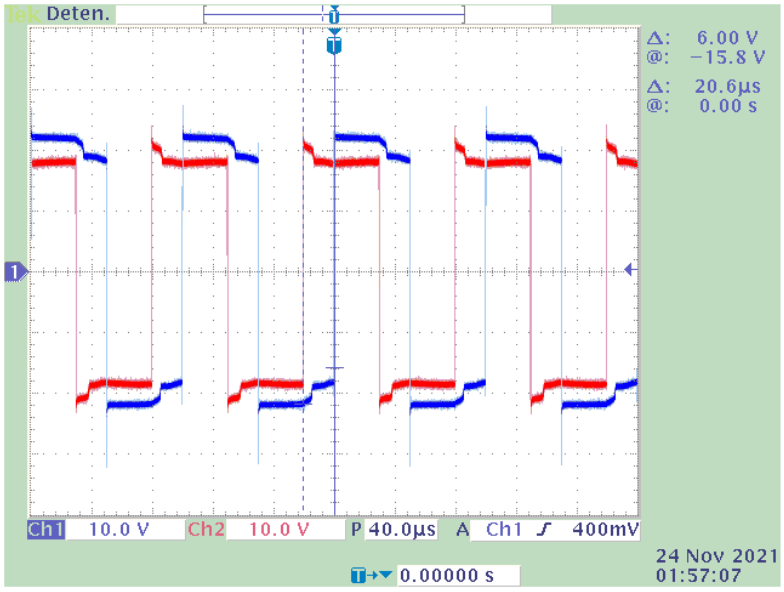

(a)

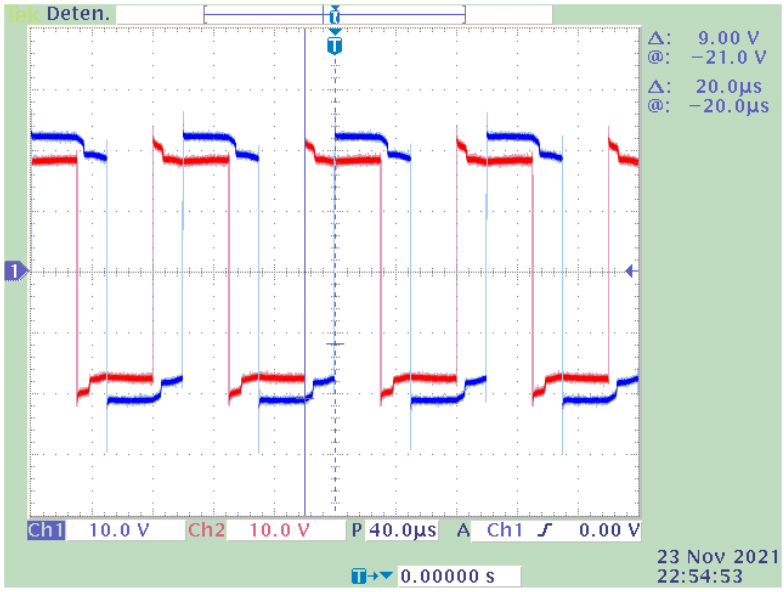

(b)

Figure 4.12: Transformer input (blue) and output (red) voltage for scenario 3: (a) PI-PBC approach, (b) Classical PI. CH1: 10V/div, CH2: 10V/div, and time base of 40 μ s.

Table 4.5: Output voltage change for both controllers when switching between scenarios occurs.

Output voltage change (%)		
Switching between scenarios	**PI-PBC**	**Classical PI**
1 - 2	0.5%	1.45%
2 - 3	0.6%	1.8%

Figs. 4.13 and 4.14 show the ability of the proposed controller to regulate the output DC voltage of the DAB device regardless of the changes in the demand of the power flow. Figs. 4.13 (a) and 4.13(b) illustrate the output voltage when the output current change from scenario 1 to scenario 2 (see Table 4.2) using the PI-PBC and the classical PI controller, respectively. While Figs. 4.14 (a) and 4.14 (b) show the output current change from scenario 2 to scenario 3 (see Table 4.2) when the PI-PBC and the classical PI controller are implemented, respectively.

In Table. 4.5, the changes in the output voltage by the application of both controllers when switching from one scenario to another are compared. Observe in Figs. 4.13 and 4.14 and in Table. 4.5 that the PI-PBC controller has a better performance than the classical PI controller since the output voltage changes are lower (around 0.6% in the worst case) when it is used. This behavior is mainly due to the fact that due to its PI - PBC structure, that converges faster to the desired equilibrium point.

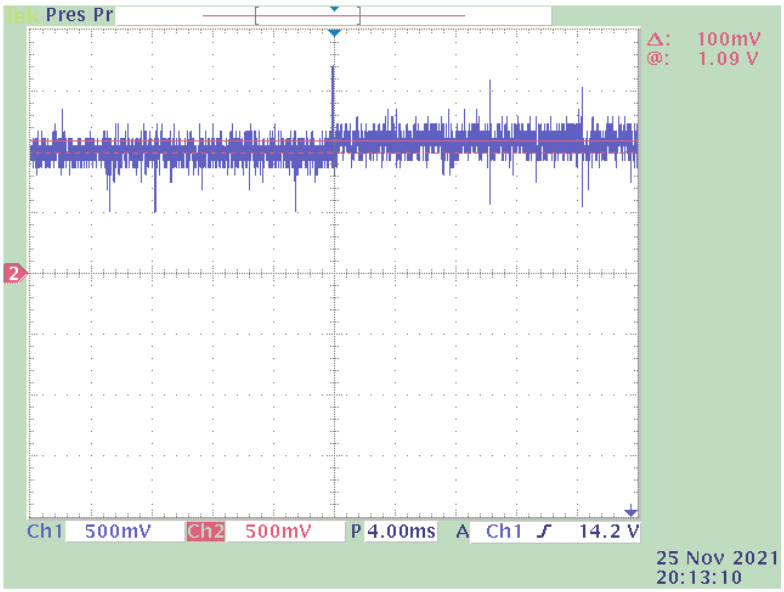

(a)

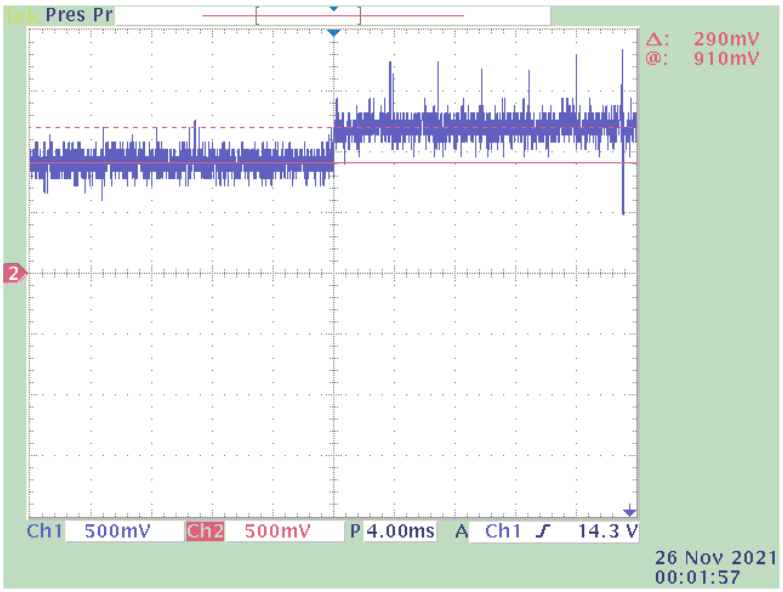

(b)

Figure 4.13: Output voltage for change between scenarios 1 and 2: (a) PI-PBC approach, (b) Classical PI. CH1: DAB output voltage (500mV/div), and time base of 4ms

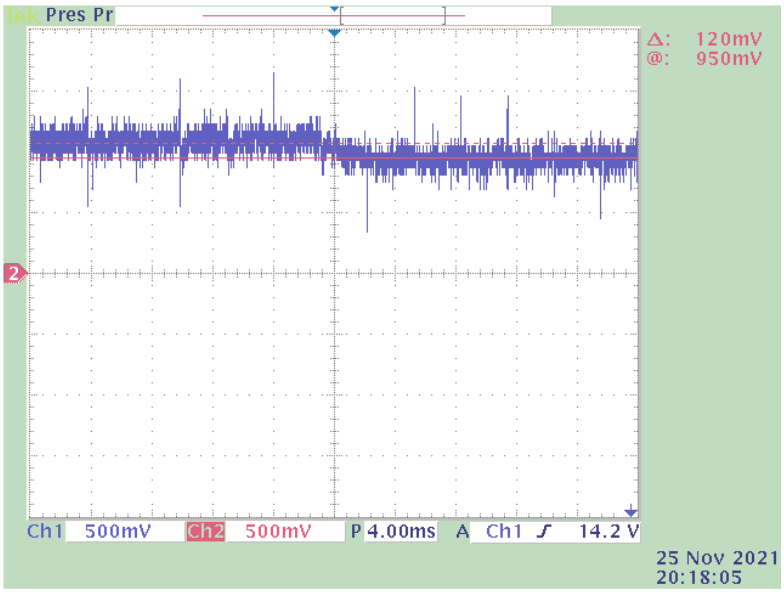

(a)

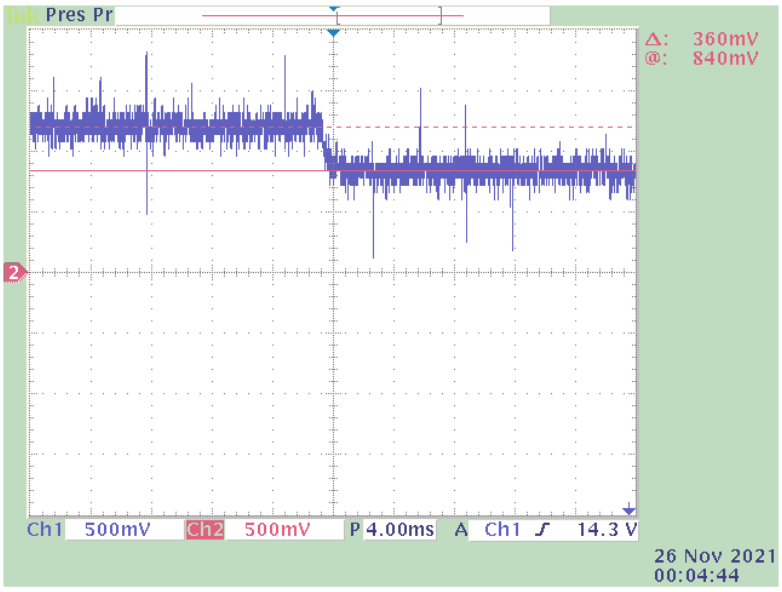

(b)

Figure 4.14: Output voltage for change between scenarios 2 and 3: (a) PI-PBC approach, (b) Classical PI. CH1: DAB output voltage (500mV/div), and time base of 4ms

Chapter 5

Conclusions

This project proposed a PI-PBC approach to regulate the power flow in the DAB, as a part of the SST. The proposed approach allowed controlling the DAB output current for any desired reference considering a specific power demand and maintaining a safe output voltage. The proposed controller was validated using simulation and experimental results under different operating conditions. In addition, the proposed controller was also compared to the conventional PI controller, where a comparison between overshoots, settling times in the output current, and its steady-state error were provided to validate the advantages of the proposed method, which had a better performance than the classical PI controller.

It was observed that overshoots, the settling time, and the steady-state error of the output current were decreased when the PI-PBC controller was implemented by 15 %, 2 ms, and 6 % in the worst-case, respectively, concerning when the classical PI was used. It is important to highlight that the PI-PBC controller proposed in this work makes the DAB model's behavior passive in the closed-loop since the DAB model is represented as a Hamiltonian port system, which maintains stability in the closed-loop. This was also supported by the analysis of the bode diagrams, where the PI-PBC approach obtained a phase margin of -112^o (from 180^o boundary) and a gain margin equal to 8.11 dB, while the classical PI obtained values -82.3^o (from 180^o boundary) and -21dB, respectively.

Future work will include the other stages of the SST with their respective controllers with techniques such as Model Predictive Control and other adaptive control techniques based on algorithmic system identification.

Bibliography

[1] B. Zeng, J. Zhang, X. Yang, J. Wang, J. Dong, and Y. Zhang, "Integrated planning for transition to low-carbon distribution system with renewable energy generation and demand response," *IEEE Transactions on Power Systems*, vol. 29, no. 3, pp. 1153–1165, 2013.

[2] C. Kang, T. Zhou, Q. Chen, J. Wang, Y. Sun, Q. Xia, and H. Yan, "Carbon emission flow from generation to demand: A network-based model," *IEEE Transactions on Smart Grid*, vol. 6, no. 5, pp. 2386–2394, 2015.

[3] W. E. S. W. A. Rashid, P. J. Ker, M. Z. B. Jamaludin, M. M. A. Gamel, H. J. Lee, and N. B. Abd Rahman, "Recent development of thermophotovoltaic system for waste heat harvesting application and potential implementation in thermal power plant," *IEEE Access*, vol. 8, pp. 105 156–105 168, 2020.

[4] J. Lorente de la Rubia, "Estudio sobre el estado actual de las smart grids," B.S. thesis, 2011.

[5] N. Hatziargyriou, *Microgrids: architectures and control*. John Wiley & Sons, 2014.

[6] W. Linyu, W. Xue, and S. Qiang, "Cost benefit analysis of combined storage and distribution generation systems in smart distribution grid," 2015.

[7] H. Farhangi, "The path of the smart grid. ieee power energy mag 8 (1): 18–28," 2010.

[8] B. Kroposki, B. Johnson, Y. Zhang, V. Gevorgian, P. Denholm, B.-M. Hodge, and B. Hannegan, "Achieving a 100% renewable grid: Operating electric power systems with extremely high levels of variable renewable energy," *IEEE Power and energy magazine*, vol. 15, no. 2, pp. 61–73, 2017.

[9] N. Rugthaicharoencheep and M. Boonthienthong, "Smart grid for energy management on distribution system with distributed generation," in *2012 IEEE International Conference on Cyber Technology in Automation, Control, and Intelligent Systems (CYBER)*. IEEE, 2012, pp. 165–169.

[10] T. C. Dias, L. A. Roque, and P. F. Ribeiro, "Power electronics in the context of renewables, power quality and smart grids," in *2016 17th International Conference on Harmonics and Quality of Power (ICHQP)*. IEEE, 2016, pp. 170–175.

[11] W. Rodrigues, L. Morais, T. Oliveira, R. Santana, A. Cota, and W. Silva, "Analysis of solid state transformer based microgrid system," in *2016 12th IEEE International Conference on Industry Applications (INDUSCON)*. IEEE, 2016, pp. 1–6.

[12] M. A. Hannan, P. J. Ker, M. S. H. Lipu, Z. H. Choi, M. S. A. Rahman, K. M. Muttaqi, and F. Blaabjerg, "State of the art of solid-state transformers: Advanced topologies, implementation issues, recent progress and improvements," *Ieee Access*, vol. 8, pp. 19 113–19 132, 2020.

[13] X. She, A. Q. Huang, and R. Burgos, "Review of solid-state transformer technologies and their application in power distribution systems," *IEEE journal of emerging and selected topics in power electronics*, vol. 1, no. 3, pp. 186–198, 2013.

[14] R. J. G. Montoya, A. Mallela, and J. C. Balda, "An evaluation of selected solid-state transformer topologies for electric distribution systems," in *2015 IEEE Applied Power Electronics Conference and Exposition (APEC)*. IEEE, 2015, pp. 1022–1029.

[15] S. Hambridge, A. Q. Huang, and R. Yu, "Solid state transformer (sst) as an energy router: Economic dispatch based energy routing strategy," in *2015 IEEE Energy Conversion Congress and Exposition (ECCE)*. IEEE, 2015, pp. 2355–2360.

[16] M. Khazraei, V. A. K. Prabhala, R. Ahmadi, and M. Ferdowsi, "Solid-state transformer stability and control considerations," in *2014 IEEE Applied Power Electronics Conference and Exposition-APEC 2014*. IEEE, 2014, pp. 2237–2244.

[17] G. Ortiz, M. Leibl, J. Kolar, and O. Apeldoorn, "Medium frequency transformers for solid-state-transformer applications—design and experimental verification," in *2013 IEEE 10th International Conference on Power Electronics and Drive Systems (PEDS)*. IEEE, 2013, pp. 1285–1290.

[18] S. Shao, L. Chen, Z. Shan, F. Gao, H. Chen, D. Sha, and T. Dragičević, "Modeling and advanced control of dual-active-bridge dc–dc converters: A review," *IEEE Transactions on Power Electronics*, vol. 37, no. 2, pp. 1524–1547, 2022.

[19] X. She, X. Yu, F. Wang, and A. Q. Huang, "Design and demonstration of a 3.6-kV–120-V/10-kVA solid-state transformer for smart grid application," *IEEE Transactions on Power Electronics*, vol. 29, no. 8, pp. 3982–3996, 2013.

[20] T. Zhao, G. Wang, S. Bhattacharya, and A. Q. Huang, "Voltage and power balance control for a cascaded h-bridge converter-based solid-state transformer," *IEEE Transactions on Power Electronics*, vol. 28, no. 4, pp. 1523–1532, 2012.

[21] X. Yu, X. She, A. Huang, and L. Liu, "Distributed power balance strategy for DC/DC converters in solid state transformer," in *2014 IEEE Applied Power Electronics Conference and Exposition-APEC 2014*. IEEE, 2014, pp. 989–994.

[22] G. G. Facchinello, L. L. Brighenti, S. L. Brockveld, D. C. Martins, and W. M. Dos Santos, "Closed-loop operation and control strategy for the dual active half bridge ac-ac converter," in *2017 IEEE 8th International Symposium on Power Electronics for Distributed Generation Systems (PEDG)*. IEEE, 2017, pp. 1–7.

[23] L. Wang, D. Zhang, Y. Wang, B. Wu, and H. S. Athab, "Power and voltage balance control of a novel three-phase solid-state transformer using multilevel cascaded h-bridge inverters for microgrid applications," *IEEE Transactions on Power Electronics*, vol. 31, no. 4, pp. 3289–3301, 2015.

[24] F. An, W. Song, B. Yu, and K. Yang, "Model predictive control with power self-balancing of the output parallel dab dc–dc converters in power electronic traction transformer," *IEEE Journal of Emerging and Selected Topics in Power Electronics*, vol. 6, no. 4, pp. 1806–1818, 2018.

[25] Q. Xiao, L. Chen, H. Jia, P. W. Wheeler, and T. Dragičević, "Model predictive control for dual active bridge in naval dc microgrids supplying pulsed power loads featuring fast transition and online transformer current minimization," *IEEE Transactions on Industrial Electronics*, vol. 67, no. 6, pp. 5197–5203, 2020.

[26] H. Zhang, Y. Li, Z. Li, C. Zhao, F. Gao, Y. Hu, L. Luo, K. Luan, and P. Wang, "Model predictive control of input-series output-parallel dual active bridge converters based dc transformer," *IET Power Electronics*, vol. 13, no. 6, pp. 1144–1152, 2020.

[27] W. Song, N. Hou, and M. Wu, "Virtual direct power control scheme of dual active bridge dc–dc converters for fast dynamic response," *IEEE Transactions on Power Electronics*, vol. 33, no. 2, pp. 1750–1759, 2018.

[28] B. Zhao, Q. Song, W. Liu, G. Liu, and Y. Zhao, "Universal high-frequency-link characterization and practical fundamental-optimal strategy for dual-active-bridge dc-dc converter under pwm plus phase-shift control," *IEEE Transactions on Power Electronics*, vol. 30, no. 12, pp. 6488–6494, 2015.

[29] Y. Shi, R. Li, Y. Xue, and H. Li, "Optimized operation of current-fed dual active bridge dc–dc converter for pv applications," *IEEE Transactions on Industrial Electronics*, vol. 62, no. 11, pp. 6986–6995, 2015.

[30] W. Gil-González, O. D. Montoya, C. Restrepo, and J. C. Hernández, "Sensorless Adaptive Voltage Control for Classical DC-DC Converters Feeding Unknown Loads: A Generalized PI Passivity-Based Approach," *Sensors*, vol. 21, no. 19, p. 6367, 2021.

[31] M. Zhang, P. Borja, R. Ortega, Z. Liu, and H. Su, "Pid passivity-based control of port-hamiltonian systems," *IEEE Transactions on Automatic Control*, vol. 63, no. 4, pp. 1032–1044, 2018.

[32] W. J. Gil-González, A. Garces, O. B. Fosso, and A. Escobar-Mejía, "Passivity-based control of power systems considering hydro-turbine with surge tank," *IEEE Transactions on Power Systems*, vol. 35, no. 3, pp. 2002–2011, 2020.

[33] O. D. Montoya, W. Gil-González, and A. Garces, "Control for eess in three-phase microgrids under time-domain reference frame via pbc theory," *IEEE Transactions on Circuits and Systems II: Express Briefs*, vol. 66, no. 12, pp. 2007–2011, 2019.

[34] O. D. Montoya, W. Gil-González, and F. M. Serra, "Pbc approach for smes devices in electric distribution networks," *IEEE Transactions on Circuits and Systems II: Express Briefs*, vol. 65, no. 12, pp. 2003–2007, 2018.

[35] O. D. Montoya, J. E. Campillo, W. Gil-González, and A. Garces, "Integration of pv arrays in dc power grids via unidirectional boost converters: a pbc approach," in *2018 IEEE 9th Power, Instrumentation and Measurement Meeting (EPIM)*. IEEE, 2018, pp. 1–6.

[36] K. López-Rodríguez, A. Escobar-Mejía, E. Piedrahita-Echavarria, and W. Gil-González, "Passivity-based current control of a dual-active bridge to improve the dynamic response of a solid-state transformer during power and voltage variations," in *2020 IEEE 11th International Symposium on Power Electronics for Distributed Generation Systems (PEDG)*, 2020, pp. 230–235.

[37] "https://www.minenergia.gov.co/cartilla-mision-transformacion-energetica."

[38] W. McMurray, "The thyristor electronic transformer: a power converter using a high-frequency link," *IEEE Transactions on Industry and General Applications*, vol. IGA-7, no. 4, pp. 451–457, 1971.

[39] X. Yu, X. She, X. Zhou, and A. Q. Huang, "Power management for DC microgrid enabled by solid-state transformer," *IEEE Transactions on Smart Grid*, vol. 5, no. 2, pp. 954–965, 2013.

[40] A. Tong, L. Hang, G. Li, X. Jiang, and S. Gao, "Modeling and analysis of a dual-active-bridge-isolated bidirectional dc/dc converter to minimize rms current with whole operating range," *IEEE Transactions on Power Electronics*, vol. 33, no. 6, pp. 5302–5316, 2018.

[41] N. Hou, W. Song, and M. Wu, "Minimum-current-stress scheme of dual active bridge dc–dc converter with unified phase-shift control," *IEEE Transactions on Power Electronics*, vol. 31, no. 12, pp. 8552–8561, 2016.

[42] K. Zhang, Z. Shan, and J. Jatskevich, "Large-and small-signal average-value modeling of dual-active-bridge DC–DC converter considering power losses," *IEEE Transactions on Power Electronics*, vol. 32, no. 3, pp. 1964–1974, 2016.

[43] A. Tong, L. Hang, G. Li, and J. Huang, "Nonlinear characteristics of DAB converter and linearized control method," in *2018 IEEE Applied Power Electronics Conference and Exposition (APEC)*. IEEE, 2018, pp. 331–337.

[44] R. Ortega and L. P. Borja, "New results on control by interconnection and energy-balancing passivity-based control of port-hamiltonian systems," in *53rd IEEE Conference on Decision and Control*. IEEE, 2014, pp. 2346–2351.

[45] R. Ortega, A. Van Der Schaft, F. Castanos, and A. Astolfi, "Control by interconnection and standard passivity-based control of port-hamiltonian systems," *IEEE Transactions on Automatic control*, vol. 53, no. 11, pp. 2527–2542, 2008.

[46] R. Cisneros, M. Pirro, G. Bergna, R. Ortega, G. Ippoliti, and M. Molinas, "Global tracking passivity-based pi control of bilinear systems: Application to the interleaved boost and modular multilevel converters," *Control Engineering Practice*, vol. 43, pp. 109–119, 2015.

[47] O. Sprangers, R. Babuška, S. P. Nageshrao, and G. A. D. Lopes, "Reinforcement learning for port-hamiltonian systems," *IEEE Transactions on Cybernetics*, vol. 45, no. 5, pp. 1017–1027, 2015.

[48] W. Gil-González, O. D. Montoya, and A. Garces, "Control of a smes for mitigating subsynchronous oscillations in power systems: A pbc-pi approach," *Journal of Energy Storage*, vol. 20, pp. 163–172, 2018.

[49] L. Perko, "Differential equations and dynamical systems," 2013.

[50] D. González Agudelo, "Diseño y construcción de un convertidor dc-dc para un transformador inteligente," 2017.

Chapter 6

Appendices

6.1 Appendix A. Gate drivers schematic.

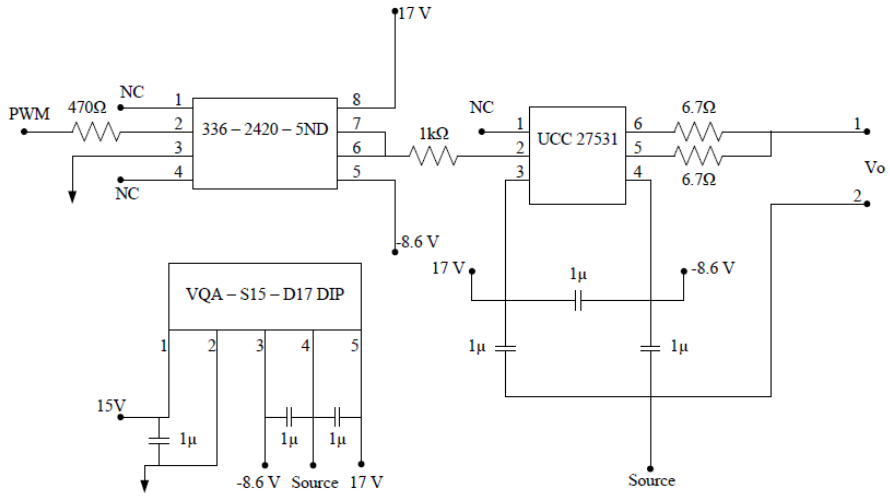

6.2 Appendix B. Voltage signal conditioning circuit.

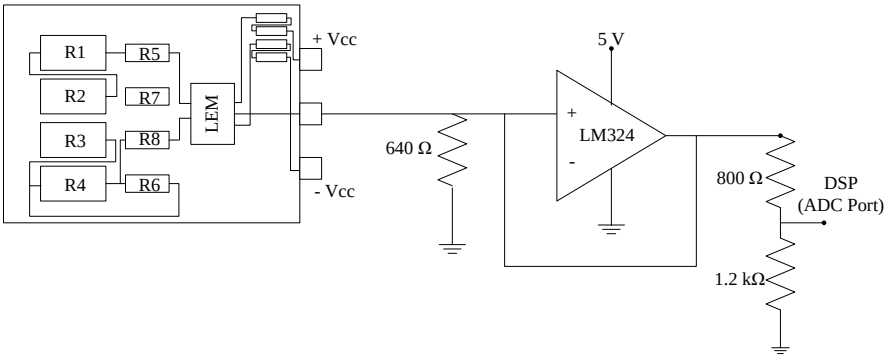

6.3 Appendix C. Current signal conditioning circuit.

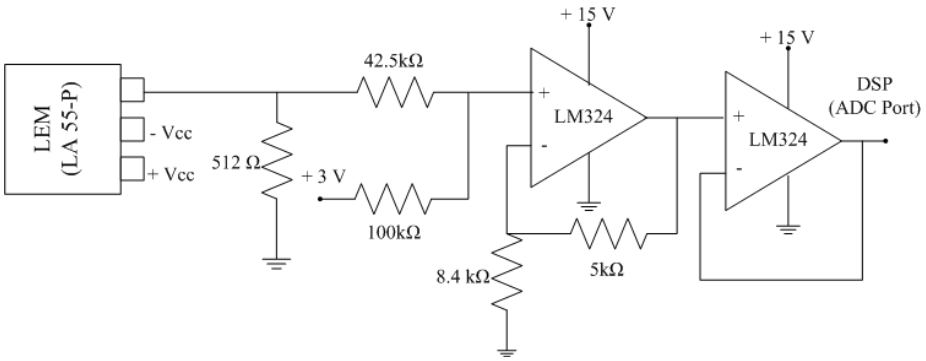

6.4 Appendix D. PI-PBC control diagram for DAB converter and C2000 processor

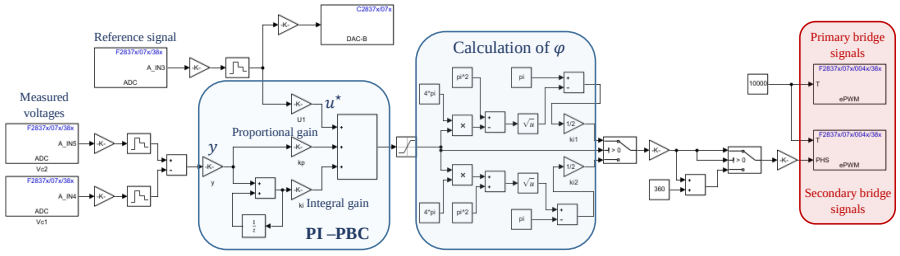

6.5 Appendix E. Classical PI control diagram for DAB converter and C2000 processor